International Communications in Heat and Mass Transfer 126 (2021) 105442

Contents lists available at ScienceDirect

International Communications in Heat and Mass Transfer

journal homepage: www.elsevier.com/locate/ichmt

Thermal convection in a cubical region saturated with a temperature-dependent viscosity fluid under the non-uniform temperature profile at vertical wall

Marina S. Astanina [a], Mohammad Ghalambaz [b,c], Ali J. Chamkha [b,c], Mikhail A. Sheremet [a,*]

[a] Laboratory on Convective Heat and Mass Transfer, Tomsk State University, Tomsk, Russia
[b] Institute of Research and Development, Duy Tan University, Da Nang 550000, Viet Nam
[c] Institute of Theoretical and Applied Research (ITAR), Duy Tan University, Hanoi 100000, Viet Nam

ARTICLE INFO

Keywords:
Free convection
Cubical cavity
Finite difference method
Variable viscosity
Non-uniform wall temperature
Vector potential functions

ABSTRACT

Convective heat transfer is a major phenomenon in different technical and natural systems. This process can be found in enclosures under the different temperature distributions at bounded walls. In this research, the thermogravitation energy transport of a non-constant viscosity medium inside a 3D region under the non-uniform or uniform temperature profile at one of the vertical walls is addressed. The opposite border is at a low constant temperature, and the remaining borders are well insulated. The control equations with the border restrictions are reduced into a non-dimensional form and then integrated by the finite difference procedures. The control characteristics are the Rayleigh number and viscosity changeable magnitude. The impacts of these characteristics on the energy transference and flow structures are studied.

1. Introduction

Process of energy transference in closed systems and blocks has a great importance in modern microelectronics. At these days, many researches of heat transfer and fluid motion in various systems can be found in [1–5]. For example, Akbarzadeh and Fardi [1] presented results of modeling of thermal convection in trapezoidal enclosures saturated with Al_2O_3/H_2O nanosuspension with the varying viscosity and heat conductivity in 2D and 3D cases. It should be noted that thermophysical properties of nanofluid in this case were depended on the nanoparticles volume fraction. Gangawane [2] investigated MHD thermogravitational convection in a warmed square chamber with Lorentz force influence and heater employing lattice Boltzmann technique. Numerical simulation was worked out for different governing parameters. It was shown that the convective flow was depended on the Lorentz force angle. Javaherdeh et al. [3] studied process of thermal convection of CuO/H_2O nanosuspension in a region having irregular borders and the magnetic field employing the dimensionless equations. One wavy wall of the cavity had a volatile high temperature while another side wall had a low temperature. Horizontal walls of the chamber were isothermal. In addition, an action of the Lorentz force was considered. The received data demonstrated that the local *Nu* was diminished owing to the magnetic influence near the hot wall. Miroshnichenko and Sheremet [4] performed a state-of-the-art analysis of turbulent free convection in different chambers by experimental and numerical methods. Different cases of energy transference were shown under the influence of various complicating factors. For examples, different boundary and initial conditions, different locations of heaters were studied. Kumar et al. [5] compared results of simulation for 2D and 3D convection of air near cylinder. The obtained data showed that the time to get the steady regime for the convective flow was depended on the geometric parameters of the cavity. Rashad et al. [6] presented results of mathematical modeling of double-diffusive convection in a closed porous chamber with different boundary conditions under the chemical reaction and heat radiation effects. The Brinkman–Forchheimer extended Darcy approach was employed for the definition of the analyzed phenomena within the porous material. The effect of governing parameters was demonstrated using the isotherms, streamlines, concentration distributions and dependences for the local *Nu* and *Sh*. The study on free convection of micropolar nanosuspension in a porous chamber with sinusoidal heating was performed by Ahmed and Rashad [7]. It was shown that the permeability ratio and the nanoparticles concentration had a huge influence on the flow structure and energy transference. The simulation of MHD thermal convection of nanofluids inside rectangular cavities was presented in [8]. Authors showed the impact of different

* Corresponding author.
E-mail address: Michael-sher@yandex.ru (M.A. Sheremet).

https://doi.org/10.1016/j.icheatmasstransfer.2021.105442

Available online 27 June 2021

Nomenclature

c	thermal capacity ($J \cdot kg^{-1} \cdot K^{-1}$)
g	gravity acceleration ($m \cdot s^{-2}$)
k	heat conductivity ($W \cdot m^{-1} \cdot K^{-1}$)
L	size of the chamber (m)
Nu	Nusselt number (−)
$\overline{Nu}$	mean Nusselt number (−)
p	static pressure (Pa)
$Pr = \frac{\mu_0}{\rho\alpha}$	Prandtl number (−)
$Ra = \frac{\rho g \beta \Delta T L^3}{\alpha \mu_0}$	Rayleigh number (−)
Sh	Sherwood number (−)
T	temperature (K)
T_c	cold border temperature (K)
T_h	hot wall temperature (K)
$T_w(\bar{z}) = T_c + (T_h - T_c)sin(\pi\bar{z}/L)$	non-uniform temperature distribution (K)
t	time (s)
$\overline{u}, \overline{v}, \overline{w}$	velocity projections ($m \cdot s^{-1}$)
u, v, w	non-dimensional velocity projections (−)
$\overline{x}, \overline{y}, \overline{z}$	coordinates (m)
x, y, z	non-dimensional coordinates (−)

Greek symbols

α	thermal diffusivity ($W \cdot m^{-2} \cdot K^{-1}$)
β	heat expansion parameter (K^{-1})
ΔT	temperature drop (K)
θ	non-dimensional temperature (−)
$\overline{\mu}(T) = \mu_0 \cdot exp\left(-\xi \frac{T-T_c}{\Delta T}\right)$	varying dynamic viscosity ($Pa \cdot s$)
μ_0	reference dynamic viscosity ($Pa \cdot s$)
$\mu = \exp(-\xi\theta)$	dimensionless dynamic viscosity (−)
ξ	viscosity varying characteristic (−)
ρ	density ($kg \cdot m^{-3}$)
τ	dimensionless time (−)
$\overline{\psi}_x, \overline{\psi}_y, \overline{\psi}_z$	vector potential functions ($m^2 \cdot s^{-1}$)
ψ_x, ψ_y, ψ_z	dimensionless vector potential functions (−)
$\overline{\omega}_x, \overline{\omega}_y, \overline{\omega}_z$	dimensional projections of vorticity vector (s^{-1})
ω_x, ω_y, ω_z	dimensionless projections of vorticity vector (−)

Subscripts

c	cooled
f	fluid
h	heated
w	wall

thermal border restrictions. Other interesting and useful results can be found in [9–13].

In the case of modeling the cooling systems for energy sources in two- and three-dimensional formulations, researchers should use the physical properties of the working medium. Often these factors play a crucial role. Such approach should be used for the description of the dependence of the heat medium characteristics on the ambient temperature and the features of heating of the cavity. It should be noted that most often researchers consider the dependence of thermophysical characteristics on temperature. Thus, Izadi et al. [14] computationally investigated free convection of Al_2O_3/H_2O nanosuspension in a chamber with energy sources and moving upper border. Viscosity, density and heat conductivity of nanosuspension were assumed to be dependent on temperature and nanoparticles volume fraction. Authors considered different locations of heaters. The results showed that the location of energy sources has a very important meaning. Rashad and El-Hakiem [15] investigated effect of temperature-dependent viscosity (linear law) and heat radiation on convection from a vertical cylinder within the porous medium. Temperature profiles, velocity and local *Nu* were shown for different governing parameters. Rani and Kim [16,17] presented results of simulation of transient thermal convection of liquid of viscosity as a function of temperature above a vertical isothermal cylinder. Authors scrutinized the influence of different viscosity and Prandtl number on heat convection in [16]. It was shown that the influence of viscosity of the working fluid and *Pr* must be taken into account for accurate prediction of the skin friction ratio. The border layer motion and heat transference of air were numerically studied in [17]. In this case the Prandtl number was considered to be constant. The obtained data indicated that the heat transfer for constant viscosity of working fluid and for variable viscosity had essential differences. Umavathi and Shekar [18] conducted study of thermogravitational convection of liquid with varying thermal characteristics including the viscosity and heat conductivity in a vertical enclosure. The differential transform technique was employed for solving the control equations. Authors noted that the growing of the viscosity resulted in a raise of the thermal convection strength whilst raising the thermal conductivity caused a decrease in the flow intensity. Thandapani et al. [19] carried out MHD unsteady convection of liquid with temperature-dependent viscosity above an isothermal upright cone. Non-dimensional variables were considered for formulation of the mathematical model. It was found that the velocity can be raised when the parameter of viscosity was increased. Further, a diminution of the viscosity of working medium resulted in an enhancement of the skin-friction ratio. Sivakumar and Sivasankaran [20] reported results of mathematical modeling of mixed convection in an oblique square chamber. The side walls of the cavity had a non-uniform distribution of temperature. The finite volume technique was used for solving of the dimensionless basic equations. Authors considered different amplitude coefficients, Richardson numbers, cavity inclination angles and phase deviations. The results demonstrated that the energy transference augmented with a rise of the region tilted angle for equal warming and cooling areas on vertical surfaces. MHD natural convection of nanofluid having variable viscosity together with thermal radiation was considered by Sheikholeslami and Rokni [21]. Isolines of temperature and stream function and *Nu* were demonstrated for various values of control characteristics including *Ra*, *Ha*, radiation parameter and nanoadditives concentration.

Currently, there are many researches of heat transfer in 3D formulation. Such tasks include usually additional factors such as energy source of different types, heated walls, and nanofluids [22–29]. For example, Ben-Cheikh et al. [22] considered 3D problem of air thermal convection and dielectric fluid ($Pr = 25$) inside a closed parallelepiped with partially cooled and heated walls. The impact of *Ra* on the fluid motion within the chamber for different working fluids (air and dielectric medium) was shown. Fusegi et al. [23] analyzed 3D thermal convection in a cube region having different thermal conditions on horizontal walls. The vertical walls were considered at a constant temperature or adiabatic. The effect of boundary conditions on flow structure inside a cavity was shown. Kwak et al. [24] numerally investigated thermogravitational convection in a cube chamber having a disk of high temperature. The obtained data presented that geometrical characteristics (the size and position) of the heated disk had a great influence on the heat transference within the region. Selimefendigil et al. [25] carried out free convection of nanofluid with two thermally insulated walls and two solid rotating blocks. The effect of the nanofluids properties, speed of rotating of cylinders and Rayleigh number on convection flow inside chamber was analyzed. Younis et al. [26] numerically studied laminar convection inside a cube with walls of constant temperature for large *Pr*. The impact of time on the liquid motion, the temperature fields and

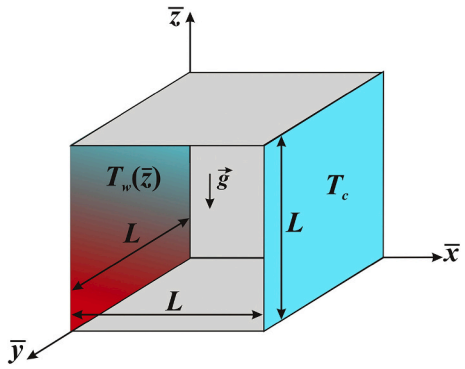

Fig. 1. Physical sketch.

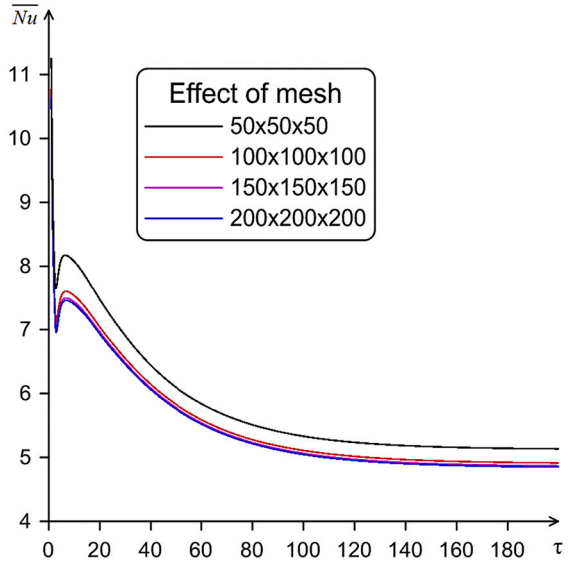

Fig. 2. Mean *Nu* at the heated wall for various meshes.

Table 1
Dependences of the velocity projections and *Nu* on the mesh parameters for $Ra = 10^5$.

	Present results for various grid sizes		[37] 62 × 62 × 62	[38] 86 × 65 × 65
	100 × 100 × 100	50 × 50 × 50		
w_{max} for $y = z = 0.5$	0.2466 (x = 0.94)	0.2471 (x = 0.94)	0.2471 (x = 0.9353)	0.2453 (x = 0.936)
u_{max} for $x = y = 0.5$	0.1389 (z = 0.15)	0.1434 (z = 0.14)	0.1468 (z = 0.1453)	0.1413 (z = 0.146)
Nu_{min} for $y = 0.5$	0.727 (z = 1.0)	0.7869 (z = 1.0)	0.7867 (z = 1.0)	0.675 (z = 1.0)
Nu_{max} for $y = 0.5$	8.072 (z = 0.08)	8.474 (z = 0.08)	7.795 (z = 0.083)	7.9669 (z = 0.0836)
$\overline{Nu}$	4.378	4.494	4.361	4.339
Nu_{mean} for $y = z = 0.5$	4.667	4.802	4.646	–

Nusselt number was analyzed. Terekhov and Ekaid [27] investigated 3D laminar convection in a chamber having two vertical surfaces of hot temperature. They examined the influence of *Ra* and the enclosure size on the energy transference. Zhu et al. [28] reported an investigation about three-dimensional convection of power-law liquid within the porous cube with adiabatic, cooled and heated walls. Different control characteristics were considered. The main motion characteristics for different values of dimensionless numbers were shown. Purusothaman et al. [29] simulated 3D thermogravitational convection of a dielectric liquid inside a cubical region having the rectangular heater. The dependences of the thermal parameters of the working zone on the determining dimensionless characteristics and the thermophysical properties of the component materials were investigated.

The current research aims to scrutinize computationally the time-dependent thermal convection of changeable viscosity medium in a cubical region under a non-uniform/uniform temperature profile at a sidewall. The analyzed medium is Newtonian thermally-conducting fluid having viscosity of temperature function. There are two cases of temperature patterns at one vertical surface, namely, constant high temperature and non-uniform temperature profile that characterizes a dependence on the vertical coordinate. An opposite wall is supposed to be cooled, while other walls are considered thermally insulated. 3D patterns of temperature, velocity and the dependences of *Nu* for various values of governing characteristics were obtained. It is necessary to highlight that results of the present study can be employed for analysis of heat exchangers, bio- and chemical reactors.

2. Basic equations

The thermogravitational convective transport and liquid motion in a three-dimensional chamber of size L presented in Fig. 1 has been considered. The liquid is thermally-conducting, Newtonian, and the Boussinesq approach is employed. The enclosure walls are impermeable with no slip boundary condition. A wall at $(\overline{x} = 0)$ is maintained at non-uniform temperature distribution $T_w(\overline{z}) = T_c + (T_h - T_c)sin(\pi\overline{z}/L)$ or at fixed hot temperature T_h, whilst the opposite surface $(\overline{x} = L)$ is at low fixed temperature T_c and other surfaces are adiabatic.

The working medium characteristics are fixed except for the density and viscosity, where the temperature correlation is used as follows $\overline{\mu}(T) = \mu_0 \cdot exp\left(-\xi \frac{T-T_c}{T_h-T_c}\right)$. The liquid circulation and energy transference in the region are assumed to be 3D. This model is an extension to the 3D system of the thermogravitational convection for the problem on energy transference by free convection in a chamber filled with a liquid of variable viscosity that has been analyzed recently by Astanina et al. [30–32].

Employing these approaches the control equations are formulated as [33]:

$$\frac{\partial \overline{u}}{\partial \overline{x}} + \frac{\partial \overline{v}}{\partial \overline{y}} + \frac{\partial \overline{w}}{\partial \overline{z}} = 0 \tag{1}$$

$$\left.\begin{aligned} \rho\left(\frac{\partial \overline{u}}{\partial t} + \overline{u}\frac{\partial \overline{u}}{\partial \overline{x}} + \overline{v}\frac{\partial \overline{u}}{\partial \overline{y}} + \overline{w}\frac{\partial \overline{u}}{\partial \overline{z}}\right) = -\frac{\partial \overline{p}}{\partial \overline{x}} + \frac{\partial}{\partial \overline{y}}\left[\overline{\mu}(T)\left(\frac{\partial \overline{u}}{\partial \overline{y}} + \frac{\partial \overline{v}}{\partial \overline{x}}\right)\right] + \\ 2\frac{\partial}{\partial \overline{x}}\left(\overline{\mu}(T)\frac{\partial \overline{u}}{\partial \overline{x}}\right) + \frac{\partial}{\partial \overline{z}}\left[\overline{\mu}(T)\left(\frac{\partial \overline{u}}{\partial \overline{z}} + \frac{\partial \overline{w}}{\partial \overline{x}}\right)\right] \end{aligned}\right\} \tag{2}$$

$$\left.\begin{aligned} \rho\left(\frac{\partial \overline{v}}{\partial t} + \overline{u}\frac{\partial \overline{v}}{\partial \overline{x}} + \overline{v}\frac{\partial \overline{v}}{\partial \overline{y}} + \overline{w}\frac{\partial \overline{v}}{\partial \overline{z}}\right) = -\frac{\partial \overline{p}}{\partial \overline{y}} + \frac{\partial}{\partial \overline{x}}\left[\overline{\mu}(T)\left(\frac{\partial \overline{u}}{\partial \overline{y}} + \frac{\partial \overline{v}}{\partial \overline{x}}\right)\right] \\ +2\frac{\partial}{\partial \overline{y}}\left(\overline{\mu}(T)\frac{\partial \overline{v}}{\partial \overline{y}}\right) + \frac{\partial}{\partial \overline{z}}\left[\overline{\mu}(T)\left(\frac{\partial \overline{v}}{\partial \overline{z}} + \frac{\partial \overline{w}}{\partial \overline{y}}\right)\right] \end{aligned}\right\} \tag{3}$$

$$\left.\begin{aligned} \rho\left(\frac{\partial \overline{w}}{\partial t} + \overline{u}\frac{\partial \overline{w}}{\partial \overline{x}} + \overline{v}\frac{\partial \overline{w}}{\partial \overline{y}} + \overline{w}\frac{\partial \overline{w}}{\partial \overline{z}}\right) = -\frac{\partial \overline{p}}{\partial \overline{z}} + \frac{\partial}{\partial \overline{x}}\left[\overline{\mu}(T)\left(\frac{\partial \overline{u}}{\partial \overline{z}} + \frac{\partial \overline{w}}{\partial \overline{x}}\right)\right] \\ +2\frac{\partial}{\partial \overline{z}}\left(\overline{\mu}(T)\frac{\partial \overline{w}}{\partial \overline{z}}\right) + \frac{\partial}{\partial \overline{y}}\left[\overline{\mu}(T)\left(\frac{\partial \overline{v}}{\partial \overline{z}} + \frac{\partial \overline{w}}{\partial \overline{y}}\right)\right] + \rho g\beta(T - T_c) \end{aligned}\right\} \tag{4}$$

$$\frac{\partial T}{\partial t} + \overline{u}\frac{\partial T}{\partial \overline{x}} + \overline{v}\frac{\partial T}{\partial \overline{y}} + \overline{w}\frac{\partial T}{\partial \overline{z}} = \alpha_f\left(\frac{\partial^2 T}{\partial \overline{x}^2} + \frac{\partial^2 T}{\partial \overline{y}^2} + \frac{\partial^2 T}{\partial \overline{z}^2}\right) \tag{5}$$

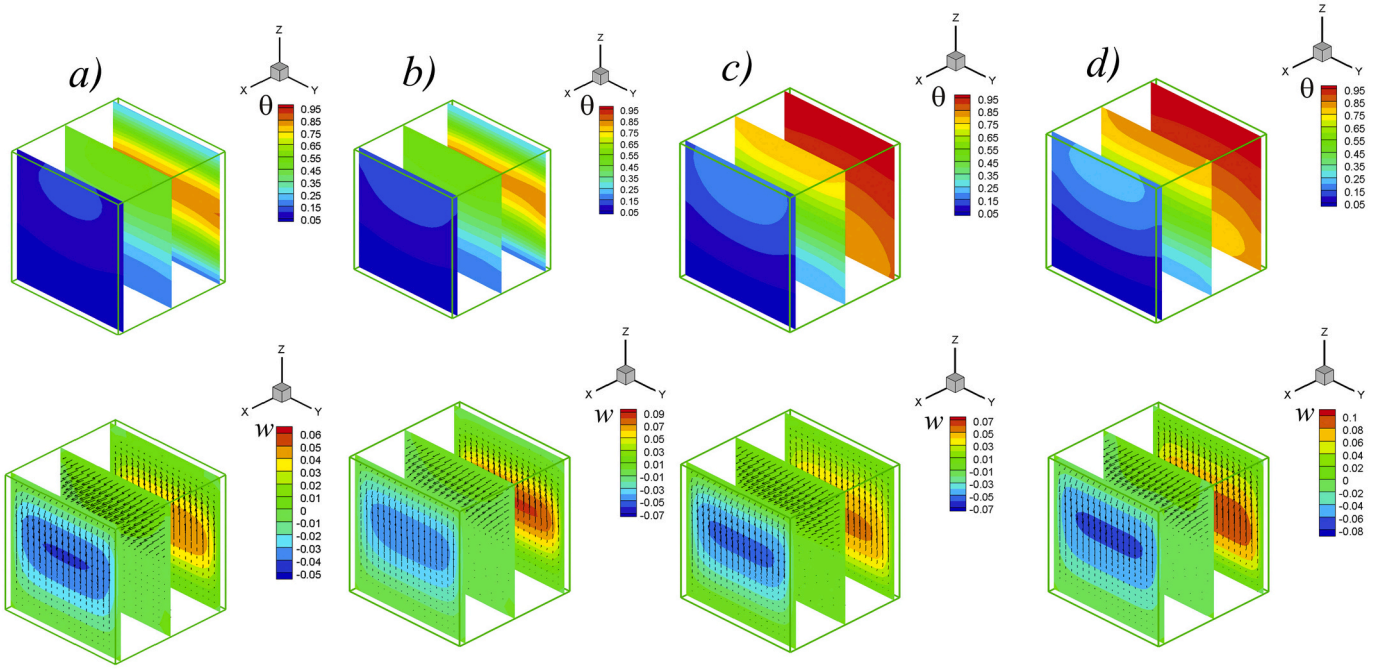

Fig. 3. The 3D maps of temperature and vertical velocity fields for $Ra = 10^4$: *a)* – non-uniform temperature distribution, $\xi = 0$, *b)* – non-uniform temperature distribution, $\xi = 1$, *c)* – constant temperature, $\xi = 0$, *d)* – constant temperature, $\xi = 1$.

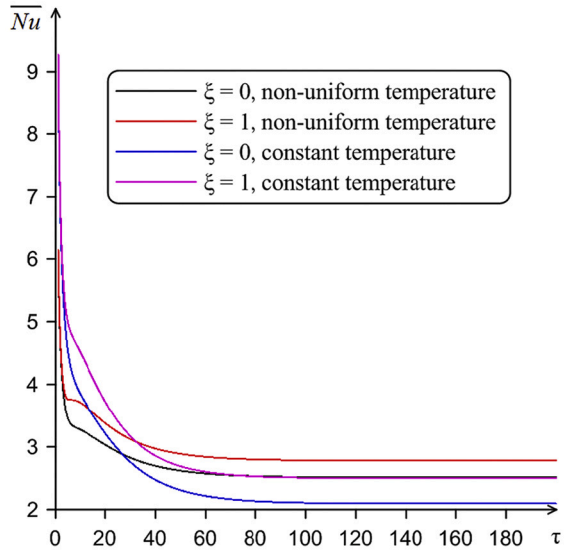

Fig. 4. Mean *Nu* at the heated border for various viscosity parameters and type of wall heating.

The formulated system of governing Eqs. (1)–(5) known as Oberbeck-Boussinesq equations includes the continuity Eq. (1), motion Eqs. (2)–(4) with the buoyancy force influence and energy Eq. (5). Eq. (1) is the continuity equation for a fluid under the Boussinesq approximation, it plays the role of an equation of state. Eqs. (2)–(4) are equations of motion for the projections of the velocity vector, reflecting the balance between inertial forces, pressure forces, friction and mass forces. The main idea of the Boussinesq approximation consists in taking into account the temperature dependence of density and as a result in this system of equations, this dependence is considered only in mass terms in Eq. (4). In addition, the viscosity of a working fluid is temperature-dependent according to an exponential function, which leads to the appearance of additional terms. Eq. (5) is an energy equation that reflects the distribution of temperature field inside the chamber.

Now, the definition of the vorticity vector $\overline{\omega}$ and potential functions $\overline{\psi}$ along with the non-dimensional parameters is employed to reduce the control equations to a dimensionless view

$$\overline{u} = \frac{\partial \overline{\psi}_z}{\partial \overline{y}} - \frac{\partial \overline{\psi}_y}{\partial \overline{z}}, \overline{v} = \frac{\partial \overline{\psi}_x}{\partial \overline{z}} - \frac{\partial \overline{\psi}_z}{\partial \overline{x}}, \overline{w} = \frac{\partial \overline{\psi}_y}{\partial \overline{x}} - \frac{\partial \overline{\psi}_x}{\partial \overline{y}}, \frac{\partial \overline{\psi}_x}{\partial \overline{x}} + \frac{\partial \overline{\psi}_y}{\partial \overline{y}} + \frac{\partial \overline{\psi}_z}{\partial \overline{z}} = 0 \tag{6}$$

vorticity projections

$$\overline{\omega}_x = \frac{\partial \overline{w}}{\partial \overline{y}} - \frac{\partial \overline{v}}{\partial \overline{z}}, \overline{\omega}_y = \frac{\partial \overline{u}}{\partial \overline{z}} - \frac{\partial \overline{w}}{\partial \overline{x}}, \overline{\omega}_z = \frac{\partial \overline{v}}{\partial \overline{x}} - \frac{\partial \overline{u}}{\partial \overline{y}} \tag{7}$$

and non-dimensional characteristics:

$$\begin{aligned} x = (\overline{x}/L), y = (\overline{y}/L), z = (\overline{z}/L), \tau = t\sqrt{g\beta(T_h - T_c)/L}, \theta = (T - T_c) \\ \Big/ (T_h - T_c), \mu = \overline{\mu} \Big/ \mu_0, u = \overline{u} \Big/ \sqrt{g\beta(T_h - T_c)L}, v \\ = \overline{v} \Big/ \sqrt{g\beta(T_h - T_c)L}, w \\ = \overline{w} \Big/ \sqrt{g\beta(T_h - T_c)L}, \psi_x \\ = \overline{\psi}_x \Big/ \sqrt{g\beta(T_h - T_c)L^3}, \psi_y \\ = \overline{\psi}_y \Big/ \sqrt{g\beta(T_h - T_c)L^3}, \psi_z \\ = \overline{\psi}_z \Big/ \sqrt{g\beta(T_h - T_c)L^3}, \omega_x \\ = \overline{\omega}_x \sqrt{L/[g\beta(T_h - T_c)]}, \omega_y \\ = \overline{\omega}_y \sqrt{L/[g\beta(T_h - T_c)]}, \omega_z \\ = \overline{\omega}_z \sqrt{L/[g\beta(T_h - T_c)]} \end{aligned} \tag{8}$$

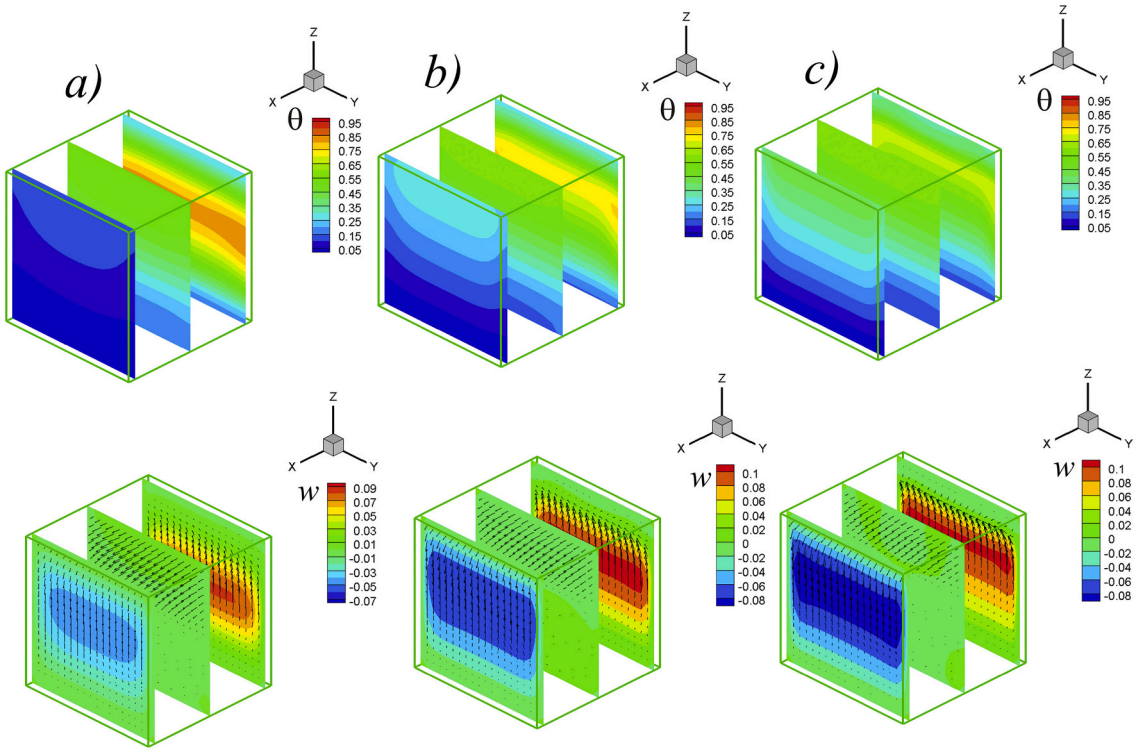

Fig. 5. The 3D maps of temperature and vertical velocity fields for $\xi = 1$ in the case of non-uniform wall temperature at different *Ra*: *a*) – $Ra = 10^4$, *b*) – $Ra = 10^5$, *c*) – $Ra = 5 \cdot 10^5$.

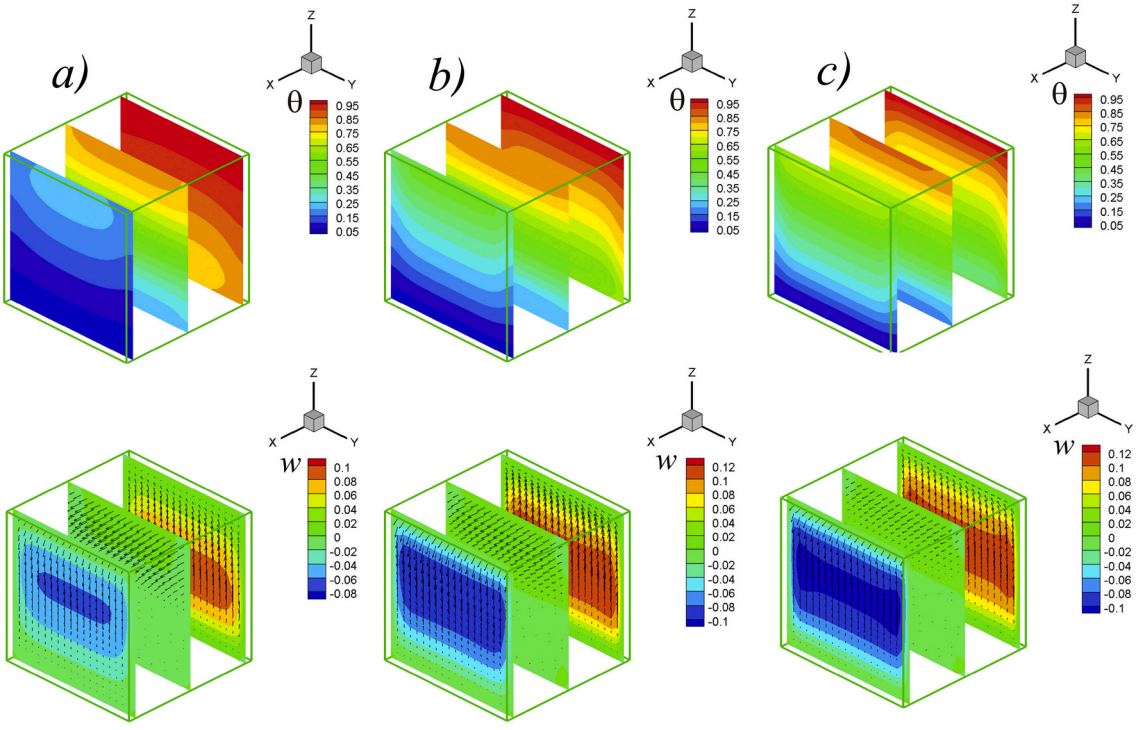

Fig. 6. 3D temperature and vertical velocity patterns for $\xi = 1$ in the case of uniform wall temperature at different *Ra*: *a*) – $Ra = 10^4$, *b*) – $Ra = 10^5$, *c*) – $Ra = 5 \cdot 10^5$.

It should be noted, that potential functions $\overline{\psi}$ characterize a relation for the velocity, namely, $\overline{V} = \mathrm{rot}(\overline{\psi})$. At the same time, the vorticity vector can be defined using the velocity vector as follows $\overline{\omega} = \mathrm{rot}\left(\overline{V}\right)$ and this vector is collinear to the vector of angular velocity of the elementary volume of the fluid as it moves in three-dimensional space. The introduction of these functions makes it possible to exclude the pressure field in the next calculations.

Finally, the control equations of convective energy transference in dimensionless vector form are:

$$\frac{\partial^2\psi_x}{\partial x^2}+\frac{\partial^2\psi_x}{\partial y^2}+\frac{\partial^2\psi_x}{\partial z^2}=-\omega_x \tag{9}$$

$$\frac{\partial^2\psi_y}{\partial x^2}+\frac{\partial^2\psi_y}{\partial y^2}+\frac{\partial^2\psi_y}{\partial z^2}=-\omega_y \tag{10}$$

$$\frac{\partial^2\psi_z}{\partial x^2}+\frac{\partial^2\psi_z}{\partial y^2}+\frac{\partial^2\psi_z}{\partial z^2}=-\omega_z \tag{11}$$

$$\left.\begin{aligned}&\frac{\partial\omega_x}{\partial\tau}+u\frac{\partial\omega_x}{\partial x}+v\frac{\partial\omega_x}{\partial y}+w\frac{\partial\omega_x}{\partial z}-\omega_x\frac{\partial u}{\partial x}-\omega_y\frac{\partial u}{\partial y}-\omega_z\frac{\partial u}{\partial z}=\\&=\sqrt{\frac{Pr}{Ra}}\left(\frac{\partial^2(\mu\omega_x)}{\partial x^2}+\frac{\partial^2(\mu\omega_x)}{\partial y^2}+\frac{\partial^2(\mu\omega_x)}{\partial z^2}\right)-\sqrt{\frac{Pr}{Ra}}\frac{\partial}{\partial x}\left(\omega_x\frac{\partial\mu}{\partial x}+\omega_y\frac{\partial\mu}{\partial y}+\omega_z\frac{\partial\mu}{\partial z}\right)+\\&+2\sqrt{\frac{Pr}{Ra}}\left[\frac{\partial v}{\partial z}\frac{\partial^2\mu}{\partial y^2}+\frac{\partial u}{\partial z}\frac{\partial^2\mu}{\partial x\partial y}-\frac{\partial w}{\partial y}\frac{\partial^2\mu}{\partial z^2}-\frac{\partial u}{\partial y}\frac{\partial^2\mu}{\partial x\partial z}+\frac{\partial^2\mu}{\partial y\partial z}\left(\frac{\partial w}{\partial z}-\frac{\partial v}{\partial y}\right)\right]+\frac{\partial\theta}{\partial y}\end{aligned}\right\} \tag{12}$$

$$\left.\begin{aligned}&\frac{\partial\omega_z}{\partial\tau}+u\frac{\partial\omega_z}{\partial x}+v\frac{\partial\omega_z}{\partial y}+w\frac{\partial\omega_z}{\partial z}-\omega_x\frac{\partial w}{\partial x}-\omega_y\frac{\partial w}{\partial y}-\omega_z\frac{\partial w}{\partial z}=\\&=\sqrt{\frac{Pr}{Ra}}\left(\frac{\partial^2(\mu\omega_z)}{\partial x^2}+\frac{\partial^2(\mu\omega_z)}{\partial y^2}+\frac{\partial^2(\mu\omega_z)}{\partial z^2}\right)-\sqrt{\frac{Pr}{Ra}}\frac{\partial}{\partial z}\left(\omega_x\frac{\partial\mu}{\partial x}+\omega_y\frac{\partial\mu}{\partial y}+\omega_z\frac{\partial\mu}{\partial z}\right)+\\&+2\sqrt{\frac{Pr}{Ra}}\left[\frac{\partial w}{\partial y}\frac{\partial^2\mu}{\partial x\partial z}-\frac{\partial w}{\partial x}\frac{\partial^2\mu}{\partial y\partial z}+\frac{\partial u}{\partial y}\frac{\partial^2\mu}{\partial x^2}-\frac{\partial v}{\partial x}\frac{\partial^2\mu}{\partial y^2}+\frac{\partial^2\mu}{\partial x\partial y}\left(\frac{\partial v}{\partial y}-\frac{\partial u}{\partial x}\right)\right]\end{aligned}\right\} \tag{14}$$

$$\frac{\partial\theta}{\partial\tau}+u\frac{\partial\theta}{\partial x}+v\frac{\partial\theta}{\partial y}+w\frac{\partial\theta}{\partial z}=\frac{1}{\sqrt{Ra\cdot Pr}}\left(\frac{\partial^2\theta}{\partial x^2}+\frac{\partial^2\theta}{\partial y^2}+\frac{\partial^2\theta}{\partial z^2}\right) \tag{15}$$

here Rayleigh number and Prandtl number are introduced as $\mathrm{R}a = \rho g\beta(T_h - T_c)L^3/(\alpha\mu_0)$and $\mathrm{Pr} = \mu_0/(\rho\alpha)$. The temperature-dependent variable dynamic viscosity is introduced as $\mu = \exp(-\xi\theta)$. This law was proposed by O. Reynolds [34]. The Rayleigh number shows the effect of a temperature gradient on the fluid flow. The Prandtl number reflects the influence of the physical properties of the working fluid on heat transfer.

The fluid is motionless for the initial moment of time and as a result vorticity vector and vector potential functions are equal to zero at initial time. Taking into account the no-slip conditions for velocity at all walls, vorticity vector components can be defined using the following definition $\overline{\omega} = \mathrm{rot}\left(\overline{V}\right)$. As for the vector potential functions, the used conditions are typical and characterize the relation between vector potential functions and velocity vector [35,36]. In addition, it is assumed that one of the vertical walls heats up according to a sinusoidal law, while the opposite wall has a constant temperature. Other surfaces are adiabatic. The dimensionless initial and boundary conditions for heat and fluid flow are introduced as:

$\tau = 0:$

$$\begin{cases}\psi_x=0,\\ \psi_y=0,\\ \psi_z=0\end{cases}\quad\begin{cases}\omega_x=0,\\ \omega_y=0,\\ \omega_z=0\end{cases}\quad\theta=0\ \text{ at }\ 0\le x,y,z\le 1$$

but $\theta = \theta_w = sin(\pi z)$ or $\theta = 1$ at $x = 0$

$\tau > 0:$

$$\begin{cases}\partial\psi_x/\partial x=0,\\ \psi_y=0,\\ \psi_z=0\end{cases}\quad\begin{cases}\omega_x=0,\\ \omega_y=-\partial w/\partial x,\\ \omega_z=\partial v/\partial x\end{cases}\quad\text{at } x=0 \text{ and } x=1,\ 0\le y,z\le 1$$

$\theta = \theta_w = sin(\pi z)$ or $\theta = 1$ at $x = 0,\ 0 \le y, z \le 1$

$\theta = 0$ at $x = 1,\ 0 \le y, z \le 1$

$\tau > 0:$

at $y = 0$ and $y = 1,\ 0 \le x, z \le 1$

$$\partial\theta\Big/\partial y=0\ \text{ and }\ \begin{cases}\psi_x=0,\\ \partial\psi_y/\partial y=0,\\ \psi_z=0\end{cases}\quad\begin{cases}\omega_x=\partial w/\partial y,\\ \omega_y=0,\\ \omega_z=-\partial u/\partial y\end{cases}$$

at $z = 0$ and $z = 1,\ 0 \le x, y \le 1$

$$\partial\theta\Big/\partial z=0\ \text{ and }\ \begin{cases}\psi_x=0,\\ \psi_y=0,\\ \partial\psi_z/\partial z=0\end{cases}\quad\begin{cases}\omega_x=-\partial v/\partial z,\\ \omega_y=\partial u/\partial z,\\ \omega_z=0\end{cases}$$

$$\left.\begin{aligned}&\frac{\partial\omega_y}{\partial\tau}+u\frac{\partial\omega_y}{\partial x}+v\frac{\partial\omega_y}{\partial y}+w\frac{\partial\omega_y}{\partial z}-\omega_x\frac{\partial v}{\partial x}-\omega_y\frac{\partial v}{\partial y}-\omega_z\frac{\partial v}{\partial z}=\\&=\sqrt{\frac{Pr}{Ra}}\left(\frac{\partial^2(\mu\omega_y)}{\partial x^2}+\frac{\partial^2(\mu\omega_y)}{\partial y^2}+\frac{\partial^2(\mu\omega_y)}{\partial z^2}\right)-\sqrt{\frac{Pr}{Ra}}\frac{\partial}{\partial y}\left(\omega_x\frac{\partial\mu}{\partial x}+\omega_y\frac{\partial\mu}{\partial y}+\omega_z\frac{\partial\mu}{\partial z}\right)+\\&+2\sqrt{\frac{Pr}{Ra}}\left[\frac{\partial v}{\partial x}\frac{\partial^2\mu}{\partial y\partial z}-\frac{\partial v}{\partial z}\frac{\partial^2\mu}{\partial x\partial y}-\frac{\partial u}{\partial z}\frac{\partial^2\mu}{\partial x^2}+\frac{\partial w}{\partial x}\frac{\partial^2\mu}{\partial z^2}+\frac{\partial^2\mu}{\partial x\partial z}\left(\frac{\partial u}{\partial x}-\frac{\partial w}{\partial z}\right)\right]-\frac{\partial\theta}{\partial x}\end{aligned}\right\} \tag{13}$$

The governing characteristics are the local Nusselt number Nu at the heated border and the mean Nusselt number $\overline{Nu}$:

$$Nu = -\left.\frac{\partial\theta}{\partial x}\right|_{x=0},\quad \overline{Nu}=\int_0^1\int_0^1 Nu\,dydz \tag{16}$$

This parameter characterizes the intensity of heat transfer between a working fluid and a solid surface.

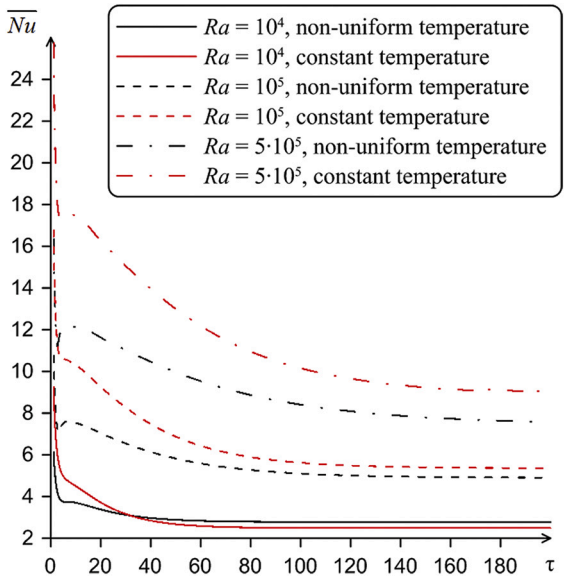

Fig. 7. Mean *Nu* at the heated border for various *Ra* and various heating of cavity for $\xi = 1$.

3. Numerical procedures

The finite difference technology has been used for the solution of the main Eqs. (9)–(15) with additional restrictions using the structured uniform mesh. The relations of parabolic kind (12)–(15) were integrated by Samarskii locally 1D technique [30–33]. The approximation of the convective terms has been performed by the monotonic Samarskii algorithm [30–33]. Diffusion terms have been reduced using the central differences. The received set of difference relations has been worked out by the Thomas method. The equations of elliptic type (9)–(11) were reduced by the central differences. The ultimate discretized relations were resolved iteratively by the over-relaxation technique.

The mesh independence validation has been carried out for $\xi = 1$, $Pr = 7.0$, and $Ra = 10^5$. The impact of different selected grid dimensions on the mean *Nu* at the hot border is demonstrated in Fig. 2. Taking into account the results of Fig. 2 the uniform mesh of $100 \times 100 \times 100$ elements was adopted for the basic simulation. The jump in the mean *Nu* at the initial time presented in this figure can be explained by the transition between the thermal conduction mode when the mean *Nu* decreases with time owing to diminution of the thermal gradient at this vertical surface and the heat convection mode when the surrounding fluid becomes hotter and ascends along this surface. A periodic temperature law characterizes an appearance of maximum temperature at the middle of this wall while the temperature decreases from the middle till the upper and lower ends of this surface. Such temperature distribution also reflects the mentioned jump in the average Nusselt number at initial time level when various fluxes can interact at this time level. Further raise in time illustrates the mean *Nu* increment owing to internal mixing of the working fluid whilst the development of convective flow characterizes an achievement of the steady state.

The created program has been validated employing the available results from literature [37,38] for the problem of thermal convection inside a differentially warmed 3D enclosure. Table 1 demonstrates the velocity projections and average *Nu* for various mesh parameters. In addition, detailed validation of the developed 3D computational code has been performed previously and presented in [30].

4. Results and analysis

The convective heat transfer and natural convection circulation in the 3D enclosure are analyzed in this section. Computational analysis is reported for $Ra = 10^3$–$5 \cdot 10^5$, $Pr = 7.0$, viscosity varying characteristic ($\xi = 0$, 1), and non-dimensional time ($0 \le \tau \le 200$). Impacts of these characteristics on the liquid motion and energy transference have been scrutinized. The maps of the vector potential functions and temperature and distributions of mean *Nu* are demonstrated in Figs. 3–7 for a combination of the non-dimensional control parameters.

Fig. 3 presents 3D patterns of vertical velocity component and temperature for various heating models of vertical surface and various viscosity parameters. In any case, the obtained results clearly illustrate the region of heating of the cavity on one of the vertical surfaces. A temperature minimum is found on the opposite border of the chamber. Convective flows are generated near the heated side wall. The fluid flow with cold temperature is located in the bottom part of the cabinet, whilst the hot liquid flow rises higher. The transition from a liquid with a fixed viscosity (Fig. 3*a*, *c*) to a liquid with a changeable viscosity (Fig. 3*b*, *d*) is reflected in the enhancement of convective motion and energy transference for any type of cavity heating.

The dependence of mean *Nu* at heated surface of chamber for various heating, viscosity parameter and $Ra = 10^4$ is demonstrated in Fig. 4. At the initial stages of time, the heat exchange occurs more intensively for the mode of constant warming of the border, and the Nusselt number reaches large values in comparison with sinusoidal distribution of temperature. A rise of time results in a reduction of the Nusselt numbers for any magnitudes of the control characteristics. The maximum value of the considered integral parameter in the stationary flow ($\tau = 200$) is achieved for the mode of a liquid with variable viscosity with non-uniform distribution of temperature. Moreover, in the mode of fixed surface temperature, the employing of a medium with varying viscosity also results in an augmentation of *Nu* at the heated border. The same effect of variable viscosity for natural convection problems (in 2D case) was shown earlier in [30].

Fig. 5 illustrates 3D patterns of θ and *w* of variable viscosity fluid for various magnitudes of *Ra* in the mode of non-uniform heating of chamber. A rise of *Ra* is reflected in the enhancement of the energy transference process in the cavity. The fluid flow rate increases significantly with increasing *Ra* from 10^4 (Fig. 5*a*) to $5 \cdot 10^5$ (Fig. 5*c*). Almost all the heat from the heated wall is redistributed in the cavity and transferred to the environment due to the cooling effect of the opposite surface. In the case of isothermal surface (Fig. 6), increasing the Rayleigh number has a similar effect on convective fluid flows. Magnitudes of the velocity component for constant heating are higher than for the sinusoidal temperature distribution.

Fig. 7 reflects an influence of *Ra* and wall heating effect for $\xi = 1$ on the mean *Nu* at hot surface of the cavity. As it was noted above, a jump in *Ra* results in a growth of energy transference strength within the region. This is especially noticeable for a region having a uniformly warmed wall (red lines). Moreover, the differences in the Nusselt values increase with Rayleigh number growth.

5. Conclusions

In this study the data of numeral simulation of transient convective energy transference of the fluid with variable viscosity in the cubical enclosure having hot vertical wall of non-uniform/uniform temperature distribution have been presented. The impact of the viscosity parameter, Rayleigh number and type of wall heating effect on energy transport and liquid circulation has been illustrated via the distributions of isotherms, vertical velocity component and mean *Nu* at the hot wall. Comparison between two types of wall temperature patterns of vertical surface shows maximum energy transference in the cabinet for constant temperature. More intensive energy removal from the hot surface can be achieved for temperature-dependent viscosity liquid for high *Ra*.

Declaration of Competing Interest

None.

Acknowledgement

This work was supported by the Russian Science Foundation (Project No. 17-79-20141).

References

[1] P. Akbarzadeh, A.H. Fardi, Natural convection heat transfer in 2D and 3D trapezoidal enclosures filled with nanofluid, J. Appl. Mech. Tech. Phys. 59 (2) (2018) 292–302.
[2] K.M. Gangawane, MHD free convection in a partially heated open-ended square cavity: effect of angle of magnetic field and heater location, Int. J. Appl. Comput. Math. 5 (63) (2019).
[3] K. Javaherdeh, M. Moslemi, M. Shahbazi, Natural convection of nanofluid in a wavy cavity in the presence of magnetic field on variable heat surface temperature, J. Mech. Sci. Technol. 31 (4) (2017) 1937–1945.
[4] I.V. Miroshnichenko, M.A. Sheremet, Turbulent natural convection heat transfer in rectangular enclosures using experimental and numerical approaches: a review, Renew. Sust. Energ. Rev. 82 (2018) 40–59.
[5] A. Kumar, J.B. Joshi, A.K. Nayak, P.K. Vijayan, 3D CFD simulation of air-cooled condenser-I: natural convection over a circular cylinder, Int. J. Heat Mass Transf. 78 (2014) 1265–1283.
[6] A.M. Rashad, S.E. Ahmed, M.A. Mansour, Effects of chemical reaction and thermal radiation on unsteady double diffusive convection, Int. J. Num. Methods Heat Fluid Flow 24 (5) (2014) 1124–1140.
[7] S.E. Ahmed, A.M. Rashad, Natural convection of micropolar nanofluids in a rectangular enclosure saturated with anisotropic porous media, J. Porous Media 19 (8) (2016) 737–750.
[8] M.A. Mansour, A.M. Rashad, S.E. Ahmed, MHD natural convection in a square enclosure using nanofluid with the influence of thermal boundary conditions, J. Appl. Fluid Mech. 9 (5) (2016) 2515–2525.
[9] A.A.A.A. Al-Rashed, L. Kolsi, H.F. Oztop, A. Aydi, E.H. Malekshah, N. Abu-Hamdeh, M.N. Borjini, 3D magneto-convective heat transfer in CNT-nanofluid filled cavity under partially active magnetic field, Phys. E: Low-dimens. Syst. Nanostruct. 99 (2018) 294–303.
[10] J.R. Lee, On the three-dimensional effect for natural convection in horizontal enclosure with an adiabatic body: review from the 2D results and visualization of 3D flow structure, Int. Commun. Heat Mass Transf. 92 (2018) 31–38.
[11] S. Shami, M. Sajid, T. Javed, Impact of complex wavy surface on natural convection flow in micropolar fluid, Num. Methods Part. Differ. Equat. (2020), https://doi.org/10.1002/num.22669.
[12] F.M. Azizul, A.I. Alsabery, I. Hashim, Heatlines visualisation of mixed convection flow in a wavy heated cavity filled with nanofluids and having an inner solid block, Int. J. Mech. Sci. 175 (2020) 105529.
[13] D.T. Yaseen, M.A. Ismael, Analysis of power law fluid-structure interaction in an open trapezoidal cavity, Int. J. Mech. Sci. 174 (2020) 105481.
[14] M. Izadi, A. Behzadmehr, M.M. Shahmardan, Effects of discrete source-sink arrangements on mixed convection in a square cavity filled by nanofluid, Korean J. Chem. Eng. 31 (1) (2014) 12–19.
[15] A.M. Rashad, M.A. El-Hakiem, Effect of radiation on non-Darcy free convection from a vertical cylinder embedded in a fluid-saturated porous medium with a temperature-dependent viscosity, J. Porous Media 10 (2) (2007) 209–218.
[16] H.P. Rani, C.N. Kim, Transient free convection flow over an isothermal vertical cylinder with temperature dependent viscosity, Korean J. Chem. Eng. 25 (1) (2008) 34–40.
[17] H.P. Rani, C.N. Kim, A numerical study on unsteady natural convection of air with variable viscosity over an isothermal vertical cylinder, Korean J. Chem. Eng. 27 (3) (2010) 759–765.
[18] J.C. Umavathi, M. Shekar, Combined effect of variable viscosity and thermal conductivity on free convection flow of a viscous fluid in a vertical channel using DTM, Meccanica 51 (2016) 71–86.
[19] E. Thandapani, A.R. Ragavan, G. Palani, MHD free convection flow over an isothermal vertical cone with temperature dependent viscosity, Thermophys. Aeromech. 19 (4) (2012) 615–628.
[20] V. Sivakumar, S. Sivasankaran, Mixed convection in an inclined lid-driven cavity with non-uniform heating on both sidewalls, J. Appl. Mech. Tech. Phys. 55 (4) (2014) 634–649.
[21] M. Sheikholeslami, H.B. Rokni, Magnetic nanofluid natural convection in the presence of thermal radiation considering variable viscosity, Eur. Phys. J. Plus 132 (238) (2017).
[22] N. Ben-Cheikh, A. Campo, N. Ouertatani, T. Lili, Three-dimensional study of heat and fluid flow of air and dielectric liquids filling containers partially heated from below and entirely cooled from above, Int. Commun. Heat Mass Transf. 37 (2010) 449–456.
[23] T. Fusegi, J.M. Hyun, K. Kuwahara, A numerical study of 3D natural convection in a cube: effects of the horizontal thermal boundary conditions, Fluid Dynam. Res. 8 (1991) 221–230.
[24] D.B. Kwak, J.H. Noh, S.J. Yook, Natural convection flow around heated disk in cubical enclosure, J. Mech. Sci. Technol. 32 (5) (2018) 2377–2384.
[25] F. Selimefendigil, H.F. Oztop, Mixed convection of nanofluids in a three-dimensional cavity with two adiabatic inner rotating cylinders, Int. J. Heat Mass Transf. 117 (2018) 331–343.
[26] O. Younis, J. Pallares, F.X. Grau, Transient natural convection cooling of a high Prandtl number fluid in a cubical cavity, Meccanica 46 (2011) 989–1006.
[27] V.I. Terekhov, A.I. Ekaid, Three-dimensional laminar convection in a parallelepiped with heating of two side walls, High Temp. 49 (6) (2011) 874–880.
[28] Q.Y. Zhu, Y.J. Zhuang, H.Z. Yu, Three-dimensional numerical investigation on thermosolutal convection of power-law fluids in anisotropic porous media, Int. J. Heat Mass Transf. 104 (2017) 897–917.
[29] A. Purusothaman, K. Murugesan, A.J. Chamkha, 3D modeling of natural convective heat transfer from a varying rectangular heat generating source, J. Therm. Anal. Calorim. 138 (2019) 597–608.
[30] M.S. Astanina, M.A. Sheremet, J.C. Umavathi, Unsteady natural convection with temperature-dependent viscosity in a square cavity filled with a porous medium, Transp. Porous Media 110 (2015) 113–126.
[31] M.S. Astanina, M.A. Sheremet, J.C. Umavathi, Unsteady natural convection in a partially porous cavity having a heat-generating source using local thermal non-equilibrium model, Int. J. Num. Methods Heat Fluid Flow 29 (6) (2019) 1902–1919.
[32] M.S. Astanina, M.M. Rashidi, M.A. Sheremet, G. Lorenzini, Effect of porous insertion on convective energy transport in a chamber filled with a temperature-dependent viscosity liquid in the presence of a heat source term, Int. J. Heat Mass Transf. 144 (2019) 118530.
[33] N.S. Gibanov, M.A. Sheremet, Natural convection in a cubical cavity with different heat source configurations, Therm. Sci. Eng. Progress 7 (2018) 138–145.
[34] O. Reynolds, On the theory of lubrication and its application to Mr. Beauchamp tower's experiments including an experimental determination of the viscosity of olive oil, Philos. Trans. R. Soc. Lond. 177 (1886) 157–234.
[35] K. Aziz, J.D. Hellums, Numerical solution of three-dimensional equations of motion for laminar natural convection, Phys. Fluids 10 (1967) 314–324.
[36] G.J. Hirasaki, J.D. Hellums, A general formulation of the boundary conditions on the vector potential in three dimensional hydrodynamics, Q. Appl. Math. 16 (1968) 331–342.
[37] T. Fusegi, J.M. Hyin, K. Kuwahara, A numerical study of 3D natural convection in a differently heated cubical enclosure, Int. J. Heat Mass Transf. 34 (1991) 1543–1557.
[38] O.A. Bessonov, V.A. Brailovskay, S.A. Nikitin, V.I. Polezhaev, Three- dimensional natural convection in a cubical enclosure: a benchmark numerical solution, in: G. de Vahl Davis, E. Leonardi (Eds.), Int. Symposium on Advances in Computational Heat Transfer, 26–30 May 1997 Cesme, Begell House, Inc, 2020, pp. 157–165.